Applicability of Genetic Algorithms to Reconstruction of Projected Data from Ultrasonic Tomography

Kodali S. P.,
Indian Institute of Technology Kanpur
Kanpur Genetic Algorithms Laboratory
Department of Mechanical Engineering
+91-512-2597668
kodalisp@iitk.ac.in

Sunith Bandaru,
Indian Institute of Technology Kanpur
Kanpur Genetic Algorithms Laboratory
Department of Mechanical Engineering
+91-512-2597668
sunithb@iitk.ac.in

Deb K.,
Indian Institute of Technology Kanpur
Kanpur Genetic Algorithms Laboratory
Department of Mechanical Engineering
+91-512-2597205
deb@iitk.ac.in

Prabhat Munshi,
Indian Institute of Technology Kanpur
Department of Mechanical Engineering
+91-512-2597243
pmunshi@iitk.ac.in

N.N.Kishore,
Indian Institute of Technology Kanpur
Department of Mechanical Engineering
+91-512-2597049
nnk@iitk.ac.in

KanGAL Report Number 2008003

ABSTRACT

In this paper simulation studies of the ultrasound computerized tomography (CT) technique employing time of flight data is presented. An enhanced genetic algorithm based reconstruction technique is proposed that is capable of detecting multiple types of inclusions in the test specimen to be reconstructed. It is assumed that the physical properties of the inclusions are known a priori. The preliminary results of our algorithm for a simple configuration are found to be better than those reported with MART1. In addition to being able to identify inclusions of different materials, both the shape and location of the inclusions could be reconstructed using the proposed algorithm. The results are found to be consistent and satisfactory for a wide range of grid sizes and geometries of inclusion(s). Based on the regression analysis an empirical relation between the number of unknowns and the reconstruction time is found which enables one to predict the reconstruction time for higher resolutions.

Keywords

Genetic algorithms, applications, ultrasonic tomography, reconstruction, time of flight, block crossover.

1. INTRODUCTION

Ultrasonic tomography (UT) has been in use for a long period now and offers the most convenient method for flaw detection in a material. However other methods have surpassed it in common usage owing to the inherent property of an acoustic wave to bend in a non-homogenous medium. Still when the material of test specimen and inclusions are known to have approximately uniform characteristics, UT provides an easy and cost effective way of reproducing the shape, size and location of the inclusion. Acoustic wave attenuation and time of flight are two reconstruction parameters which can be used for this purpose. Simulated time of flight data without considering ray bending is used in the present work.

Popular reconstruction methods for projection data obtained from UT include transform methods like Convolution back projection (CBP) and series expansion methods represented by algebraic reconstruction technique (ART) and its variant multiplicative algebraic reconstruction technique (MART). The main difference between the two being that, in the former the distribution is kept continuous until the very end and only the final formulas are discretized for computational implementation whereas, in the latter the problem is discretized at the very beginning by superimposing a grid on the specimen and assuming constant physical properties within each pixel of the grid. The tomogram obtained using transform methods gives a gradation of the physical property being reconstructed over the material-inclusion boundary rather than a clear cut edge which can be produced by any discrete tomography technique. Further, transform methods require complete set of projection data for reconstruction which may not be available in a number of practical problems.

Discretization, as one may think, is not always an approximation of the problem at hand. In fact there are several cases like when the number of atoms in each line of a crystal lattice is to be determined, where continuous tomographic techniques cannot be used, because the unknown image is binary instead of real-valued. A lattice cell either contains one or no atom, but it certainly will not contain a fraction of an atom. This additional constraint transforms the problem from analytic to combinatorial and here lies the motivation for using genetic algorithms.

Genetic algorithms are search and optimization techniques based on the dynamics of natural selection and genetics. First proposed

by John Holland in 1975, genetic algorithms are now being put to use in a wide range of applications. Their versatility is due to the fact that they can handle continuous as well as discrete problems in almost the same way provided we can define a basis for establishing the superiority of one member in the search space over another. Also since they work with a population rather than a single initial point global convergence is most certainly ensured. Algebraic reconstruction techniques on the other hand, suffer from their inherent possibility of getting entrapped in a local optimum.

Though optimization methods in tomography like entropy optimization were suggested as far back as 1983 [1], GAs to our knowledge were applied only in the late 90^s with Kihm and Lyons [2] using them in optical tomography. The accuracy of the image however depended on the choice of the elementary distribution functions which is known a priori only in certain cases. Curtis and Snieder [3] used GAs to reduce the ill conditionality of inverse problems in general. The first direct approach to tomography using GAs was by Bichkar and Ray [4] for the reconstruction of circular and elliptical objects of known intensities placed on a known uniform background. Delsanto [5] demonstrated the applicability to ultrasound tomography using simulated time of flight data. It is this work we intend to extend through this paper to the reconstruction of specimens with multiple inclusions both in number and the material of inclusions.

The process of reconstruction consists of two major steps, the first is acquisition of time of flight data and the second is using the acquired data to reconstruct the specimen under consideration. The following sections convey the adopted approach; in section 2 we explain the simulation procedure adopted for acquiring time of flight data, in section 3 we discuss the GA based reconstruction algorithm developed, in section 4 we present our results and finally we present the conclusions in section 5.

2. DATA ACQUISITION

In this work we have simulated the time of flight data required for reconstruction following the procedure outlined by Delasanto [5]. The specimen under consideration is represented as a square matrix grid of certain integer values with each value corresponding to one type of material. In our work value 0 corresponds to base material, and values 1 and 2 correspond to two different inclusion materials. Figure 1 shows the internal computer representation and its visual display for a representative specimen with two types of inclusions.

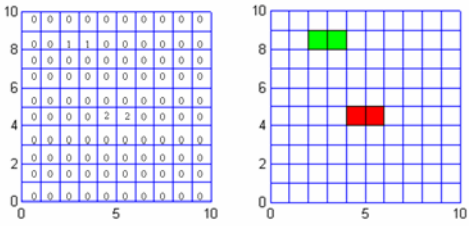

Figure 1. A representative sample used for simulating the time of flight data

To gather the time of flight data the specimen is assumed to be placed on the test bed with a number of ultrasound sources and detectors arranged at different locations. In our study we use the modified cross-hole geometry [6] configuration and the sources and detectors are placed equally distributed on four sides of specimen. For practical considerations one pair of a set of sources and detectors is used in different configurations to ensure that the entire specimen is covered by ultrasound rays. Table 1 gives the various placement configurations considered.

Table 1. Source-detector placement configurations

Configuration	Sources position	Detectors position
LFT-TOP	Along left edge	Along top edge
TOP-RGT	Along top edge	Along right edge
RGT-BOT	Along right edge	Along bottom edge
BOT-LFT	Along bottom edge	Along left edge
LFT-RGT	Along left edge	Along right edge
TOP-BOT	Along top edge	Along bottom edge

For a given configuration from each of the source one ray travels to each of the detectors giving us time of flight data equal to the product of number of sources and number of detectors. Depending on how many of the configurations given in Table 1 are used total number of simulated times of flight obtained equals to the product of number sources, number of detectors and the number of configurations. For example with six sources, six detectors and six configurations we obtain a total of 216 times of flight data, which essentially is the input to our reconstruction algorithm. The ray coverage for this case is illustrated in Figure 2.

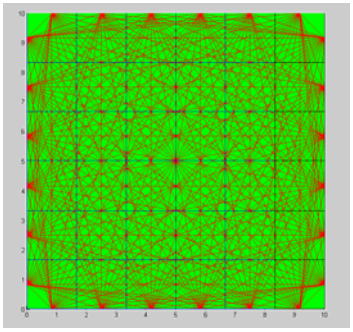

Figure 2. Ray coverage for 6 sources, and 6 detectors arranged in 6 configurations.

The simulated time of flight for a ray originating from j-th source and terminating at the k-th detector is estimated according to the relation,

$$simulated\_tof(j,k) = \sum_{m=1}^{M} \frac{l_m}{v_m}$$

Where,

M = Number of cells through which the ray passes,
l_m = Length of the ray intercepted by m-th cell,
v_m = Velocity of propagation of ultrasound through the m-th cell (depends on the material corresponding to that cell).

As mentioned at the start of this section a maximum of three different materials have been considered, one for representing

the base material and two for inclusion materials. However the same can be extended easily to consider a higher number of materials.

3. RECONSTRUCTION ALGORITHM

Using the simulated time of flight data we perform the reconstruction process. Traditionally the reconstruction process is performed either by the inverse Fourier transform approach or the iterative techniques that are represented by ART and its variants. A third technique not so popularly used is the optimization approach. In our work the reconstruction process is addressed with a genetic algorithm developed for the purpose. Specifically, we are looking for a particular distribution of the inclusion(s) which best agrees with the simulated data obtained. The flowchart of the algorithm used is shown in Figure 3. In the following sections we describe the salient features of the algorithm.

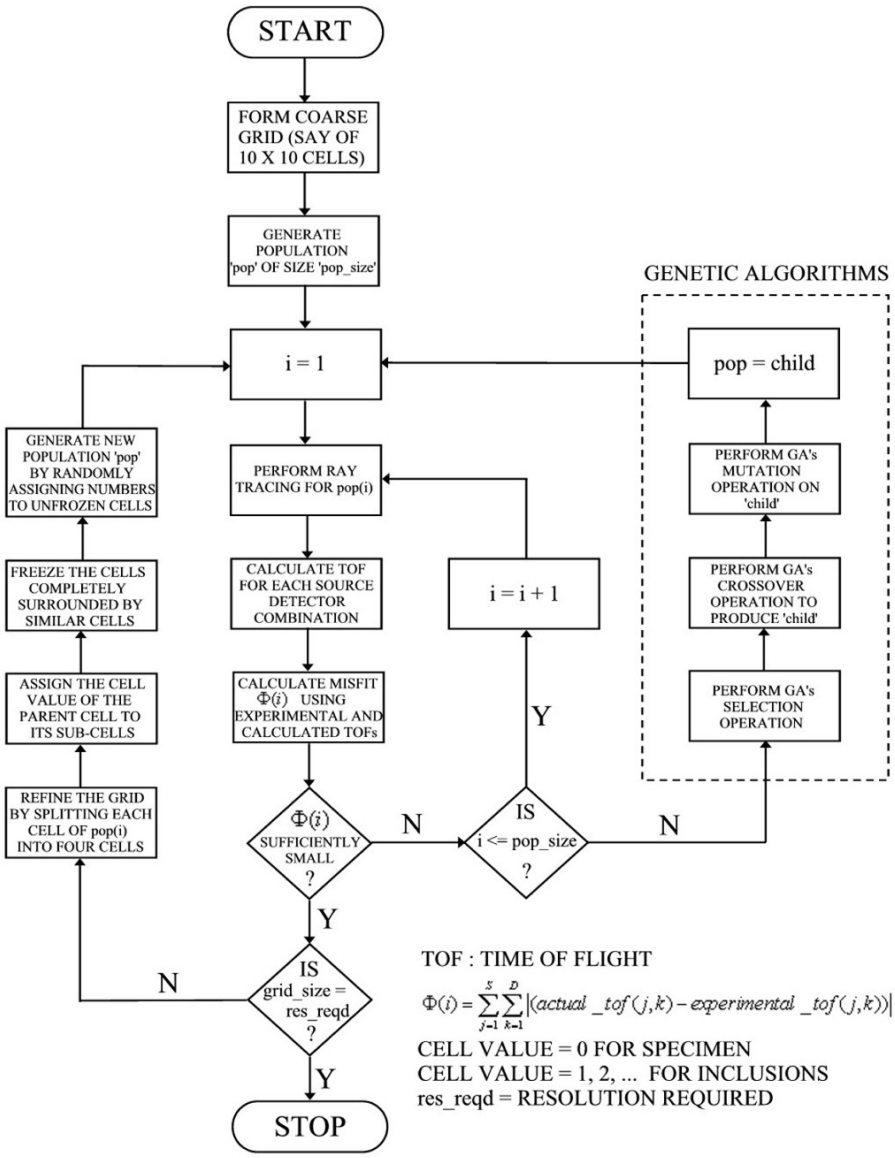

Figure 3. Flowchart of the GA based reconstruction algorithm

3.1 Overview

To begin with, we generate a population of solutions with random distributions of some numbers of a required grid-size. We use the term 'grid-size' to denote number of rows or columns of the matrix representing a potential solution to the problem in hand. For the final solution the grid-size should match with the required resolution. The initial randomly generated distribution population has a coarse grid-size and is refined during the reconstruction process. The idea is to proceed in steps towards the solution. The best possible solution with a relatively coarser initial grid serves as a seed for the next finer grid. Thus the core structure of the inclusions is identified in the initial steps while the later ones refine their boundaries. The initial coarse grid is so chosen that its repeated doubling gives a value near, preferably equal to the final resolution required.

3.2 Fitness Evaluation

Each population member is now evaluated for its fitness. Fitness is defined here as the sum of absolute differences between the simulated time-of-flight (TOF) data for the test specimen and the population member under consideration. The following definition of misfit (fitness function) is used which is to be minimized. As we are using simulated data, the term 'experimental_tof' in the definition shown in the flowchart (Figure 3) is replaced with the term 'simulated_tof' here.

$$\Phi(i) = \sum_{j=1}^{S}\sum_{k=1}^{D}\left|actual\_tof(j,k) - simulated\_tof(j,k)\right|$$

Where, $\Phi(i)$ = Misfit of *i*-th population member

S = Number of Sources

D = Number of Detectors

3.3 Selection

Using the fitness evaluated as above, selection operation is performed to emphasize good population members in mating pool from which a child population is created. Selection operation is accomplished following tournament selection procedure [7]. Pairs of population members are picked randomly and the best population member in terms of fitness is put in the mating pool.

3.4 Crossover

The selection process performed does not create new solutions but only ensures that good solutions are emphasized. To create new solutions, crossover operation is performed on the population members in the mating pool created by selection operation. New solutions (children) are created by interchanging or swapping corresponding portions of the grid between two mating pool members (parents) which are selected randomly. The mating pool members as well as the location and size of portions to be swapped are picked randomly. The normal crossover operation of GA is modified to suit the two-dimensional nature of the population members in the problem at hand. Instead of creating a single random number as the crossover site, four random numbers are created (two for each corner of sub-matrix). These sub-matrices are exchanged in the subsequent 'block-crossover' operation. An example of this is shown in Figure 4.

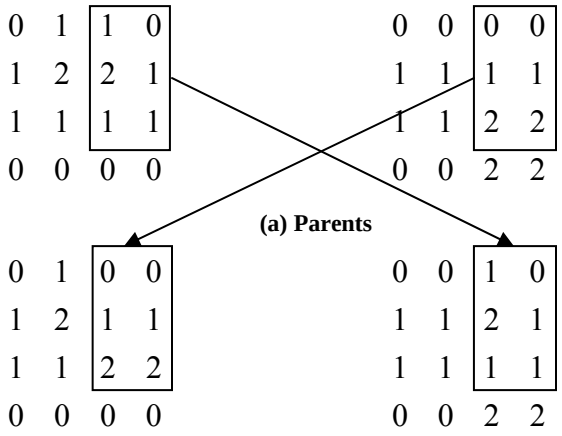

(b) Resulting Children

Figure 4. Illustration of block-crossover operation

3.5 Mutation

Two different types of mutations have been incorporated into the reconstruction algorithm. The first is the more obvious 'bitwise-mutation', where cells of the member eligible for mutation are randomly assigned values 0 or 1 or 2 other than the present value in the selected cell. The second termed 'block-mutation', finds the value that appears most number of times in the selected cell itself and its eight surrounding cells and mutates the values in all nine cells to this new value. Bitwise and block mutations are illustrated in Figure 5. During simulation runs it was found that bitwise mutations lose their efficacy for grid sizes greater than 30x30. Similarly block mutations are ineffective for lower grid sizes.

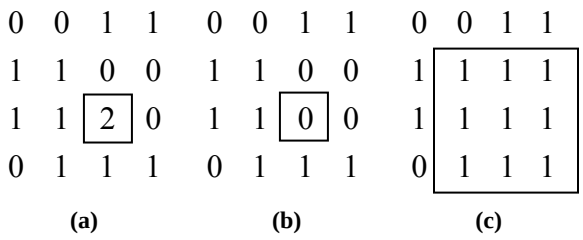

Figure 5. (a) Population member before mutation, (b) Result of bitwise-mutation, and (c) Result of block-mutation

3.6 Elite Preservation

In this step termed elite preservation, the child population obtained after mutation operation and the initial population are combined and the best of these equal to the initial population size, are picked as elites. This ensures that good solutions propagate to subsequent generations. After this the initial population is reset with elites and the GA steps discussed are repeated for a certain number of generations. The best population member from the elites obtained after desired number of generations is complete, is reported as the reconstructed solution.

3.7 Refining Coarse Solutions

The resulting solution with a coarse grid is now used to generate a new initial population with a higher grid size, say double the current grid-size. For this, each cell of the coarse grid is divided into four and given the same value as in the parent cell. Thus, each time a grid is refined the parameter 'grid-size' doubles in value.

The next step is to freeze those cells of the refined grid which correspond to the core structure of the inclusion. To identify such cells, the value in each cell is compared with those in the surrounding eight cells. If they all match, the cell under consideration is frozen. To implement this programmatically, frozen cells are assigned 10, 11, and 12 corresponding to values 0, 1, and 2 in the unfrozen state. Thus a cell with value 2 surrounded by cells with same value would be frozen by assigning a value 12. Values of cells that do not meet these criteria are unaltered.

After refinement and freezing, we obtain what we call the base-population member that serves as a seed for creating new initial population members of larger grid size. The new initial

population is created by randomly assigning values to the unfrozen cells in the base-population leaving the values in frozen cell unaltered. The base-population itself could be made a member of this new population. The GA operations are now performed on this population and the procedure is repeated till the required resolution is obtained.

3.8 Termination Criteria

The termination criteria used in our study is the number of generations per step. However, as we do not know final grid size desired by the user, we check the quality of solutions obtained with two successive grid sizes and terminate the GA if these two are similar. For larger resolutions if the above criteria are not met we continue till the projected reconstruction times as shown in Table 3 and stop.

4. RESULTS AND DISCUSSIONS

4.1 Comparison with MART

MART1 was used [8] to reconstruct a constant impulse field as shown in Figure 6 (a). The results show that though MART is capable of locating the inclusion's approximate position, it is not consistent when the shape of the inclusion is of major concern. Also this algorithm is highly dependent on the relaxation parameter λ and a proper tuning of this parameter is required for achieving good results. The same data when provided to our algorithm gave definite results, Figure 6 shows this distinction. MART algorithm required eleven transducers per edge to obtain the image in Figure 6 (b), while a better image was produced as shown in Figure 6 (c) with only 3 transducers per edge with our algorithm. This was the case with most reconstructions which shows the suitability of this new approach to limited data tomography.

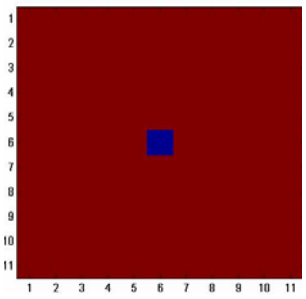

(a) Specimen used to obtain simulated time of flight data [8]

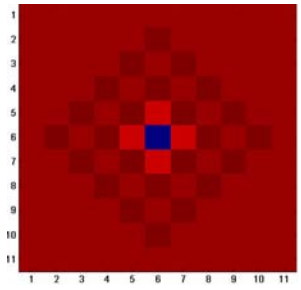

(b) Reconstructed image using MART1 [8] with λ = 0.01

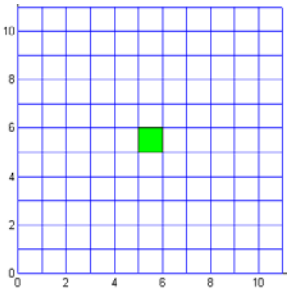

(c) Reconstructed image using proposed algorithm

Figure 6. Comparison of MART and GA reconstructed images

4.2 Reconstructed Images

In order to establish the robustness of the algorithm more than 250 simulations with combinations of different types of inclusions in terms of material, shape, size, and location of the inclusions were performed. Also the samples were reconstructed considering various resolutions required from 6x6 grids to 64x64 grids. Reconstruction results are observed to be fairly consistent for a majority of the cases analyzed. Some representative results of successful reconstructions are illustrated in Figure 7. In each of the figures shown, the left part is the visual display of the specimen to be reconstructed (used for simulating the time of flight data) while the right part is the reconstructed image. Base material is displayed in white, whereas green and red colors denote inclusions of two different materials. Figure 7(a) shows the reconstruction results for a specimen without any inclusions whereas Figures 7(b) – 7(g) show the results with different configurations considered. For each of these the sample size (SS), resolution required (RR), starting grid size (SGS), number of sources (SRC), number of detectors (DET), and number of generations per step (GEN) used are indicated.

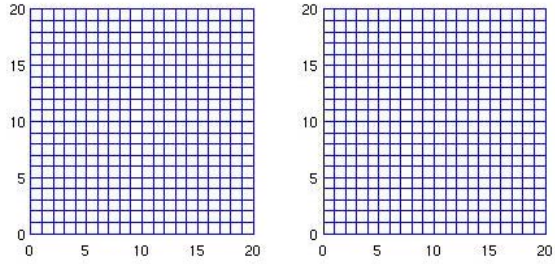

(a) SS=20, RR=20, SGS=10, SRC=7, DET=7, GEN=1000

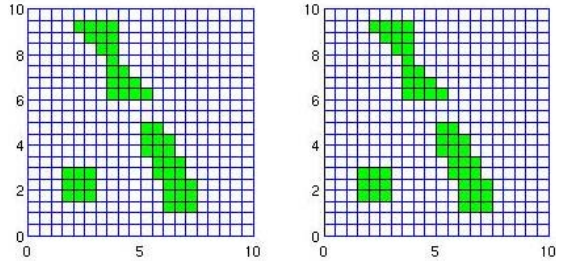

(b) SS=10, RR=20, SGS=10, SRC=7, DET=7, GEN=1000

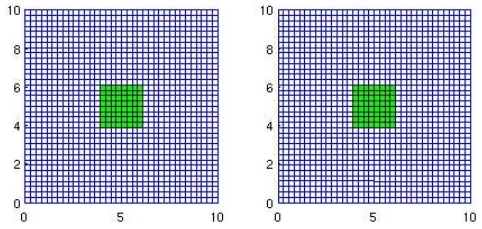

(c) SS=10, RR=36, SGS=9, SRC=12, DET=12, GEN=1000

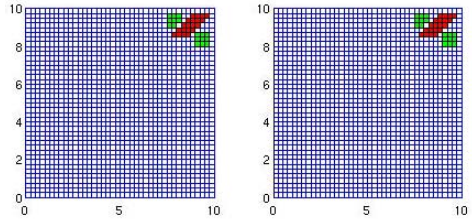

(d) SS=10, RR=40, SGS=10, SRC=13, DET=13, GEN=1000

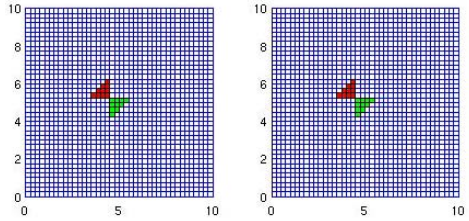

(e) SS=10, RR=40, SGS=10, SRC=13, DET=13, GEN=1000

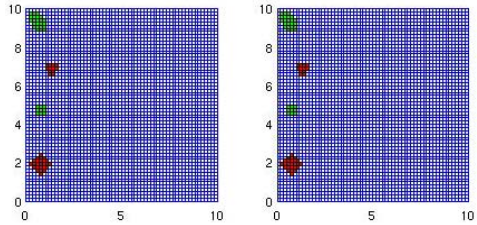

(f) SS=10, RR=60, SGS=15, SRC=19, DET=19, GEN=1000

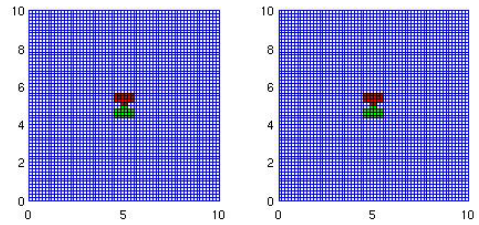

(g) SS=10, RR=60, SGS=15, SRC=19, DET=19, GEN=1000

Figure 7. Few successful reconstruction results

From our studies based on the simulation results, some of which we show in Figure 7, following parameter settings were found to yield consistent results: crossover probability of 0.8, mutation probability of 0.2, number of generations for each step equal to 1000, and a population size equal to three times the resolution required. The minimum number of sources and detectors required is such that simulated time of flight data is roughly 55 to 65 % of number of cells in final grid resolution required. Although reconstructing coarser grids required much smaller number of generations and smaller population size the goal is to estimate a common set of GA parameters that is able to perform equally well for any desired resolution.

Some simulations with arbitrarily shaped inclusions of multiple types and at many locations were performed to check the robustness of the algorithm. It is observed that while most of the inclusions were easily detected, the algorithm failed to capture the exact image in some cases with the parameter settings described above. In Figure 8 we present a few cases of these. In particular it is observed that this occurs when wave-propagation velocities through the materials considered are similar. For such situations the fitness functions values for each of the population members is very close and the algorithm cannot make definite decisions in picking up the best population members. One solution to this could be an appropriate scaling of the fitness function values before selection operation. However even for these cases our algorithm shows a trend towards the correct solution with an increase in the number of generations. Figure 9 shows the improved reconstruction results with an increase in the number of generations, for the corresponding results shown in Figure 8.

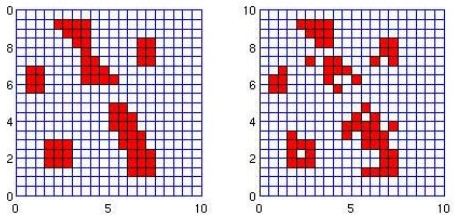

(a) SS=10, RR=20, SGS=10, SRC=7, DET=7, GEN=1000

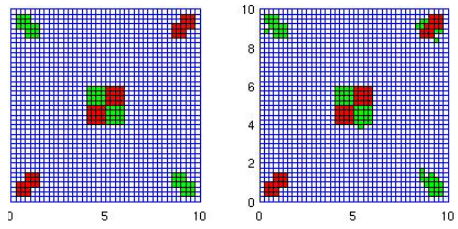

(b) SS=10, RR=40, SGS=10, SRC=13, DET=13, GEN=1000

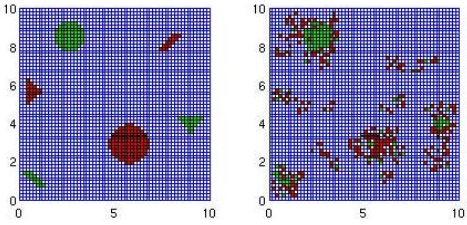

(c) SS=10, RR=60, SGS=15, SRC=19, DET=19, GEN=1000

Figure 8. Few unsuccessful reconstruction results

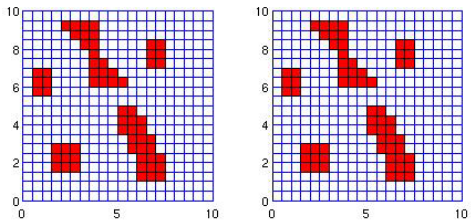

(a) SS=10, RR=20, SGS=10, SRC=7, DET=7, GEN=1500

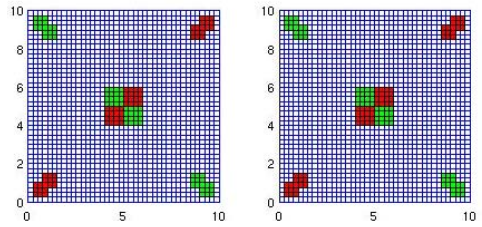

(b) SS=10, RR=40, SGS=10, SRC=13, DET=13, GEN=1500

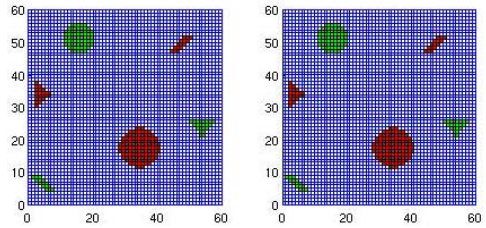

(c) SS=10, RR=60, SGS=15, SRC=19, DET=19, GEN=2500

Figure 9. Improvement in reconstruction results of Figure 8 with increase in number of generations.

4.3 Fitness History

Figure 10 shows how the fitness and mean fitness values of a population vary with increase in the GA generations.

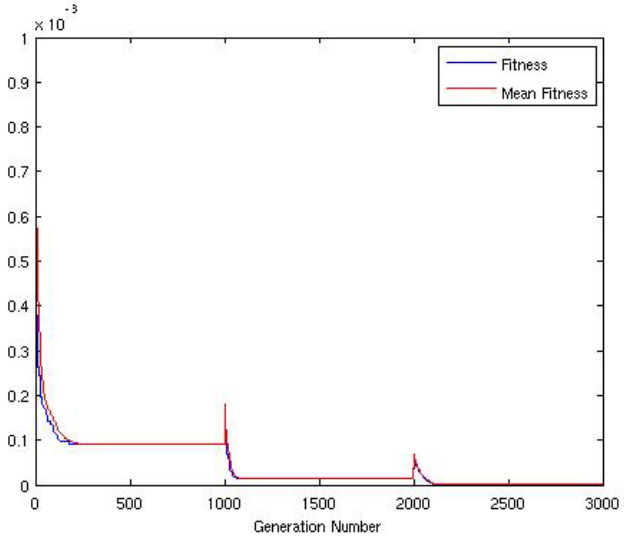

Figure 10. Fitness history for the reconstructed image in Figure 7 (c)

It can be observed that for each of the grid sizes both the fitness function and mean fitness values reach a peak and decrease rapidly followed by an almost asymptotic decrease in these values. The logic behind starting with a coarse grid initially and then refining it after a specified number of generations is well supported by these plots. If we were to use a single fine grid initially to obtain the solution, it would have taken much larger number of generations to achieve the desired solution or the solution would get stuck at a local optima with fewer generations. Observe that the rate at which the fitness decreases is very slow after the rapid decrease initially. We also observe that it is the refining of the grid and the creation of a new population of solutions by retaining the core of the solution already obtained, which drives the algorithm towards the desired solution quickly.

4.4 Reconstruction Times

All reconstructions were performed on a SUN E250 machine with 400 MHz dual processor and 1GB RAM using MATLAB7 software. In Table 2 we present the average reconstruction times recorded for reconstructing specimens with required resolutions varying from 6x6 to 64x64. The values given are averages of ten similar runs with a single inclusion of square shape covering roughly 9-10 % of the specimen area and located in the centre of the specimen. In each of the runs, a population size equal to three times the resolution required is used. Number of generations for each of the steps is specified as 1000. The crossover and mutation probabilities used are 0.8 and 0.2 respectively.

Table 2. Simulation times for various resolutions required

Final Grid Size (Resolution)	Number of Unknowns	Average Reconstruction Time (seconds)
6x6	36	9
9x9	81	22
12x12	144	41
14x14	196	201
16x16	256	169
18x18	324	244
20x20	400	413
22x22	484	649
24x24	576	639
26x26	676	1367
28x28	784	1844
32x32	1024	2878
36x36	1296	3491
40x40	1600	4594
44x44	1936	7810
48x48	2304	9815
52x52	2704	16345
56x56	3136	21452
60x60	3600	22266
64x64	4096	33258

A logarithmic plot of number of unknowns versus reconstruction times and the least squares straight line fitted through the data is shown in Figure 11.

The regression equation between the number of unknowns(x) and the reconstruction times (y) is estimated to be

$$y = 0.009(x)^{1.8057}$$

This turns out to be near quadratic and using the regression relation, we present in Table 3 the projected times for reconstruction of the samples considering larger resolutions. The projected reconstruction times can be used as termination

criteria for the algorithm when we are dealing with a given resolution.

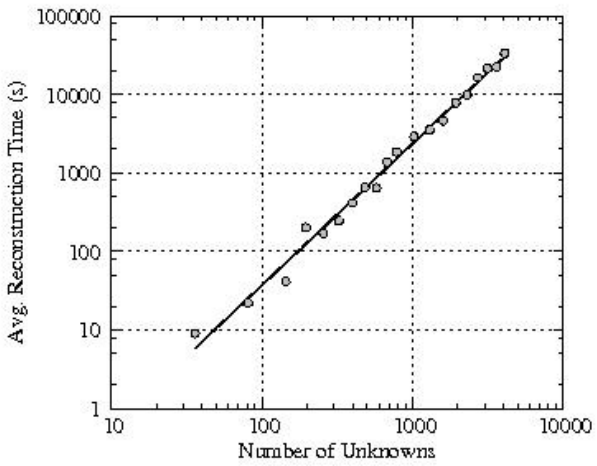

Figure 11. Log – Log plot of number of unknowns (resolution required) versus time taken for reconstruction.

Table 3. Projected reconstruction times

Grid Size (Resolution)	Number of Unknowns	Projected Average Reconstruction Time (seconds)
70x70	4900	41460
90x90	8100	102753
100x100	10000	150328
128x128	16834	385007

5. CONCLUSIONS

An established method for reconstruction of projected data from ultrasonic tomography using genetic algorithms is modified to work for multiple inclusions. The developed algorithm is tested over a wide range of grid-sizes and yielded satisfactory results in numerous simulation runs performed with different inclusion configurations. The procedure competes with long used methods like ART and MART and even surpasses MART when only a limited amount of data is available.

The effects of population sizes and number of generations were studied and suitable values for both were arrived at. It is found that for a majority of cases, a population size three times that of the final required grid size and 1000 generations were sufficient for capturing any type of arbitrarily shaped inclusions up to resolutions of 64x64. A study of the simulation times revealed logarithmically linear variation enabling us to estimate the reconstruction times for larger grid sizes.

A preliminary study on the effect of crossover and mutation probabilities showed no consistent patterns. However further investigation into the role of these operators is encouraged. One variation of the mutation operator namely, block mutation, greatly enhanced the algorithm's performance for grid sizes greater than 30x30. An explanation for this could be the ineffectiveness of mutating only a few bits in a large grid of 30x30 or more.

As can be realized from Table 3, the simulation times increase greatly with the increase in required resolution and hence parallelization of the code becomes necessary in such cases. The authors would like to emphasize that, for the algorithm to be of more practical relevance ray bending and diffraction effects must be taken into consideration. Further progress in these directions is the authors' future objective. Currently we are working on validating the proposed algorithm for real world experimental data.

6. REFERENCES

[1] Yair Censor, "Finite Series-Expansion Reconstruction Methods", Proceedings of the IEEE, Vol. 71, No. 3 (1983).

[2] Ken D. Kihm and Donald P. Lyons, "Optical Tomography using a Genetic Algorithm", Optical Society of America, Optics Letters, Vol. 21, No. 17 (1996).

[3] Andrew Curtis and Roel Snieder, "Reconditioning Inverse problems using the Genetic Algorithm and Revised Parameterization", Society of Exploration Geophysicists, Geophysics, Vol. 62, No. 4, pp. 1524-1532 (1997).

[4] R. S. Bichkar and A. K. Ray, "Tomographic Reconstruction of Circular and Elliptical Objects using Genetic Algorithm", IEEE, IEEE Signal Processing Letters, Vol. 5, No. 10 (1998).

[5] P. P. Delsanto, A. Romano, M. Scalerandi and F. Moldoveanu, "Application of Genetic Algorithms to Ultrasonic Tomography", J. Acoustical Society of America, Vol. 104, No. 3, Pt. 1 (1998).

[6] A.C. Kak and Malcolm Slaney, Principles of Computerized Tomographic Imaging, IEEE Press (1998).

[7] Kalyanmoy Deb, Optimization for Engineering Design: Algorithms and Examples", Prentice-Hall of India Pvt. Ltd. (2005).

[8] Saurabh Khare, Mayuri Razdan, Prabhat Munshi, B. V. Soma Sekhar and K. Balasubramaniam, "Defect Detection in Carbon-Fiber Composites using Lamb-Wave Tomographic Methods", American Society for Nondestructive Testing, Research in Nondestructive Evaluation, Vol. 18, Issue 2, pp. 101-119 (2007).